International Journal of Heat and Mass Transfer 139 (2019) 537–547

Contents lists available at ScienceDirect

International Journal of Heat and Mass Transfer

journal homepage: www.elsevier.com/locate/ijhmt

Heat transfer performance of sintered Cu microchannels produced by a novel method

Kaikan Diao, Yuyuan Zhao *

School of Engineering, University of Liverpool, Liverpool L69 3GH, UK

ARTICLE INFO

Article history:
Received 9 August 2018
Received in revised form 29 January 2019
Accepted 7 May 2019

Keywords:
Microchannel
Porous metal
Cu powder sintering
Heat transfer
Pressure drop

ABSTRACT

Microchannels have many thermal management applications due to their high heat transfer performance. In this paper, sintered Cu microchannels with well controlled channel diameters of 450 μm, 390 μm and 290 μm, and volume fractions of channels of 0.1, 0.2, 0.3 and 0.4, were manufactured by a new method and their pressure drops and heat transfer coefficients were compared with conventional machined Cu microchannel and porous Cu manufactured by Lost Carbonate Sintering (LCS). The pressure drops of the sintered Cu microchannels were higher than a conventional machined microchannel, but significantly lower than LCS porous Cu samples. The sintered Cu microchannels achieved a similar range of heat transfer coefficients as the LCS porous Cu, with much lower volume fractions of channels. They had higher heat transfer coefficients than the conventional machined microchannel, mainly due to the introduction of multilayers of channels in the metal matrix. Darcy-Weisbach and Sieder-Tate equations with the introduction of appropriate correcting factors can be used to estimate the pressure drop and heat transfer coefficient of the sintered Cu microchannels. There exists a strong correlation between heat transfer coefficient and pumping power.

1. Introduction

Thermal management has increasingly become a key issue in many industrial sectors in recent years. This is especially the case in electronic devices, where miniaturization of electronic components and increasing current density require more rapid and efficient heat dissipation [1,2]. There are constant needs for improvement in cooling techniques to maintain these components within the required temperature limits [3]. Among the common cooling techniques, forced convection cooling is one of the most effective processes commonly found in a variety of consumer and industrial products ranging from personal computers to avionics control systems. Heat is removed from a component and dissipated into a fluid that can be blown or pumped away to maintain favorable working temperatures in the electronic systems [3].

Micro-flow heat exchange devices have become an important thermal management solution in many applications where space is constrained [4–9]. Two micro convection flow cooling systems, namely microchannels [4,7,9] and porous metals [10–13], in particular, have recently attracted many interests in both industry and academia. Microchannel heat exchangers exhibit high heat transfer coefficients and low pressure drops [4–6,9]. However, the relatively high costs involved in manufacturing microchannels, e.g., by micro-mechanical cutting [14–16], wet and dry etching [17–21] and laser cutting [22–24], have limited their applications to more critical components. Furthermore, the channels are usually confined to the top surface due to the constraints of the manufacturing technologies, which limits the heat dissipation area available in microchannels. Porous metals, such as porous Cu manufactured by the lost carbonate sintering (LCS) process, on the other hand, have lower costs and often higher heat transfer coefficients than microchannels due to their high internal surface areas, improved conduction and convection, and turbulence-induced fluid mixing [10–13,25–28]. However, the fluid pathways in LCS porous Cu samples (Fig. 1) are formed by randomly distributed interconnected pores and are highly tortuous, posing a high resistance to fluid flow. High pumping power is required to move the working fluid through them, hindering their wider applications in thermal management [12,13,29].

Porous metals with directional pores are potentially cost-effective heat exchangers because they combine the main benefits and circumvent some of the serious drawbacks of microchannels and porous metals. Directional porous metals have unidirectional and independent channels in the metal matrix. The metal matrix gives a high thermal conductivity, the porous structure offers a

* Corresponding author.
E-mail address: yyzhao@liverpool.ac.uk (Y. Zhao).

https://doi.org/10.1016/j.ijheatmasstransfer.2019.05.020
0017-9310/

Nomenclature

A	area of the sample in contact with heat source (m^2)
A_S	total area of the channels in contact with the fluid (m^2)
D	diameter of the channels (m)
f	volume fraction of channels
f_D	Darcy friction factor
h	heat transfer coefficient of sample (W/m^2 K)
h_s	heat transfer coefficient of a single channel (W/m^2 K)
k	thermal conductivity of the fluid
L	length of sample (m)
N	number of channels
Nu	Nusselt number of sample
Nu_s	Nusselt number of a single channel
P	pumping power (W)
Pr	Prandtl number
Re	Reynolds number
U	Volume flow rate of the fluid (m^3/s)
V	volume of sample (m^3)
V_A	areal volume of channels (m)
V_C	total volume of channels (m^3)
v	flow velocity (m/s)
x	width of sample (m)
y	height of sample (m)

Greek symbols

Δp	pressure drop (Pa)
μ	dynamic viscosity (Ns/m^2)
μ_s	dynamic viscosity of the fluid evaluated at the channel wall temperature (Ns/m^2)
ρ	density of fluid (kg/m^3)

large specific surface area, and the directional pores or channels provide lower flow resistance than conventional porous metals [2,30–32]. One such example is the lotus-type porous metals produced by unidirectional solidification of metals utilizing metal-gas eutectic systems [33,34]. However, the lengths of the directional pores in lotus-type porous metals by this method are short and not uniform [2,10,33]. They have to be cut into thin sections and then re-assembled in order to form continuous open channels. Another example is an array of directional micro-holes in an aluminum alloy fabricated by inserting carbon fibers into molten aluminum and pulling them out after the solidification of the melt [35]. This method produces directionally porous Al with a relatively low volume fraction of channels. Hokamoto et al. [36] manufactured cylindrical directional channels by welding together many copper pipes using an explosive compaction method. This is an expensive method and is only suitable for fabricating channels of large diameters.

This paper introduces a new low-cost method to manufacture copper microchannels with controlled diameter and quantity of well aligned open channels. The key parameters characterizing the overall heat transfer performance of the material, including heat transfer coefficient, pressure drop and the required pumping power, are measured and analyzed.

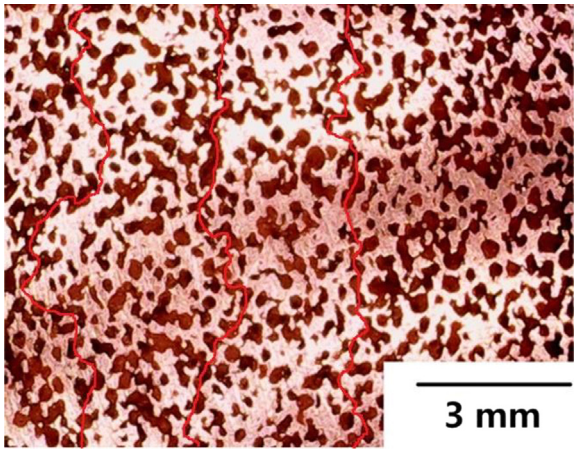

Fig. 1. Microstructure of LCS porous Cu (porosity: 0.75, pore size: 250–425 μm), illustrating typical tortuous fluid pathways.

2. Experimental

2.1. Preparation of sintered Cu microchannels

The raw materials used in fabricating the sintered Cu microchannels were a commercially pure Cu powder with a mean particle size of 20 μm and polylactic acid (PLA) fibers with three different diameters of 290 μm, 390 μm and 450 μm. The PLA fibers were first coated with a thin layer of the Cu powder using a polyvinyl alcohol (PVA) glue. At the same time, a Cu particle slurry was prepared by mixing a portion of the Cu powder with ethanol, which served as a binder. The coated PLA fibers were then embedded in the Cu particle slurry contained in a mould with dimensions of 20 mm × 35 mm × 5 mm, with the fibers placed along the longitudinal direction, equally interspaced and parallel to each other. The slurry-fibre mixture was heated in a furnace in atmosphere at 650 °C for 30 min, where the Cu particles were partly oxidized and sintered together while the PVA binder was evaporated and the PLA fibers were decomposed. The resultant CuO microchannel body was finally heated in vacuum (<4 × 10^{-2} mBar) at 1000 °C for 6 h to be reduced to Cu, forming a Cu microchannel. The Cu microchannel sample was cut by an EDM machine into 30 mm long, ensuring completely open channels. Fig. 2 shows the typical transverse cross sections of the sintered Cu microchannels, with channel diameters of 450 μm (a), 390 μm (b) and 290 μm (c), and a typical longitudinal cross section of the Cu microchannel with a channel diameter of 290 μm (d). The porosity of the sintered Cu matrix, measured by the quantitative stereology method, is approximately 15%, i.e., the density of the sintered Cu matrix is about 85% of dense Cu.

To facilitate comparison between different porous materials, two parameters, namely volume fraction of channels and areal volume of channels, are used to characterise the capacities of the sintered Cu microchannels for the transportations of fluids and heat. Volume fraction of channels, f, is the ratio of the total volume of the channels to the volume of the sample, or the ratio of the total cross-sectional area of the channels to the cross-sectional area of the sample perpendicular to the channel direction:

$$f = \frac{V_c}{V} = \frac{N\frac{\pi}{4}D^2}{xy} \quad (1)$$

where V_c is the total volume of the channels, V is the volume of the sample, N is the number of channels in the sample, D is the diameter of the channels, x is the width of the sample and y is the height

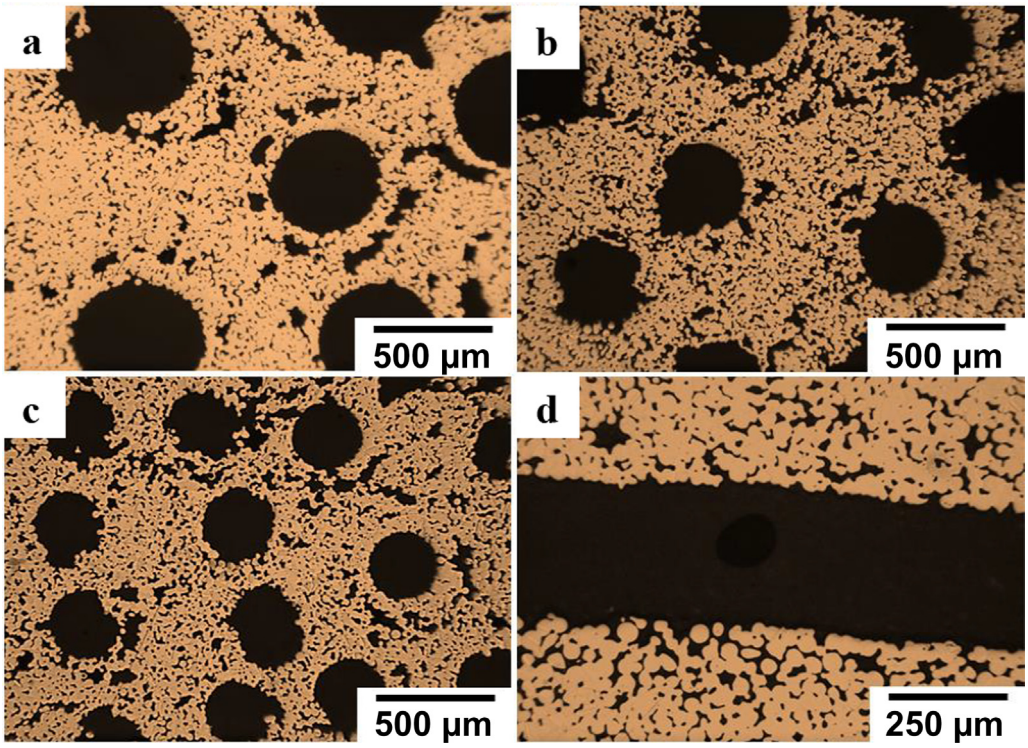

Fig. 2. Typical microstructure of the sintered Cu microchannels. Transverse cross sections with channel diameters of (a) 450 μm, (b) 390 μm and (c) 290 μm and (d) longitudinal cross section with a channel diameter of 290 μm.

of the sample, with *xy* being the cross-sectional area of the sample perpendicular to the channel direction. *f* is also the porosity of the porous material, if the channels are treated as pores.

Areal volume of channels, V_A, is the total volume of the channels divided by the surface area of the sample in contact with the heat source, i.e., the cross-sectional area of the sample perpendicular to the heat flow. It is also equal to the total cross-sectional area of the channels divided by the width of the sample perpendicular to the channel direction and can be determined by:

$$V_A = \frac{V_c}{A} = \frac{N\frac{\pi}{4}D^2}{x} \tag{2}$$

where *A* is the area of the sample in contact with the heat source, i.e., *xL*, with *L* being the length of the microchannel sample in the channel direction.

While volume fraction of channels is sufficient to quantify the capacity of the sintered Cu microchannels for passage of fluids, it is not suitable for describing the heat transfer capability, because heat dissipation is also dependent on the arrangement of the channels in relation to the heat flux. Areal volume of channels needs to be used as a basis for comparing heat transfer performance between different porous media.

For each channel diameter, four sintered Cu microchannel samples with $f = 0.1$, 0.2, 0.3 and 0.4 ($V_A = 0.5$, 1.0, 1.5 and 2.0 mm, respectively) were manufactured. The different volume fractions were achieved by adjusting the number of channels in the samples. Table 1 shows the number of channels for each combination of volume fraction, *f*, and diameter, *D*, of channels.

2.2. Measurements of pressure drop and heat transfer coefficient

The experimental apparatus (Fig. 3) and the procedures used to measure the pressure drop and heat transfer coefficient of the sintered Cu microchannel samples were nearly the same as that described in [13]. The only difference is that a new copper heating block was used, with the distance between the two temperature measurement spots increased to 80 mm so that the heat flow to the sample, and accordingly the heat transfer coefficient, could be determined with a much improved accuracy. The sintered Cu microchannel samples were machined to 30 mm in length (*L*), 20 mm in width (*x*) and 5 mm in height (*y*), as shown in Fig. 4.

Table 1
Number of channels to achieve a volume fraction *f* for each channel diameter *D*.

Channel diameter	Volume fraction *f*			
D (μm)	0.1	0.2	0.3	0.4
290	151	303	454	606
390	84	168	251	335
450	63	126	189	252

The heat block was machined by a precision milling machine and the sintered Cu microchannel samples were cut by an EDM machine. Their geometrical parameters were measured by a caliper for ten times, giving an error less than 0.05 mm. The accuracies of the pressure gauges and the thermocouples are 0.01 bar and 1 °C, respectively. The maximum errors of the pressure drop per unit length and the heat transfer coefficient, obtained by uncertain analysis, were 0.47 bar/m and 1.1 kW/m^2 K, respectively.

3. Results and discussion

3.1. Pressure drop

Fig. 5 shows the variations of pressure drop per unit length with flow rate for the sintered Cu microchannels with different volume fractions of channels (0.1, 0.2, 0.3 and 0.4) and different channel diameters (450 μm, 390 μm and 290 μm). It shows that the pressure drop increases linearly with flow rate and decreases with volume fraction of channels. For the volume fraction of channels and

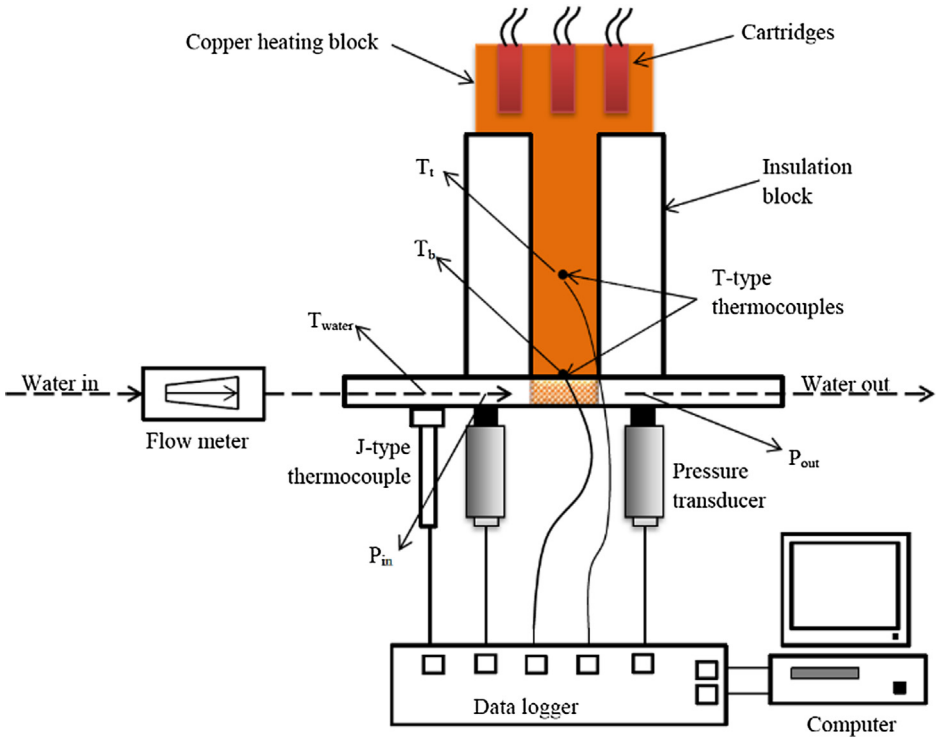

Fig. 3. Schematic of experimental apparatus used for pressure drop and heat transfer coefficient measurements.

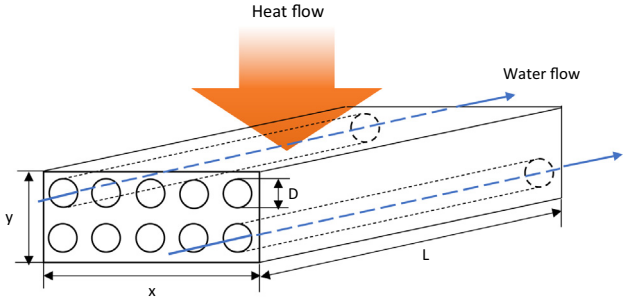

Fig. 4. Schematic diagram of a sintered Cu microchannel sample showing heat flow and water flow directions relative to the direction of the channels.

flow rate, the smaller the channel diameter, the higher the pressure drop.

Fig. 6 compares the pressure drops of the sintered Cu microchannels with those of the LCS porous Cu [37] and a conventionally machined Cu microchannel [38], as a function of flow velocity. The flow velocity is determined by dividing the volume flow rate of the fluid by the total cross-sectional area of the channels. The LCS porous Cu samples [37] had a pore size of 250–425 μm and different porosities of 57%, 65% and 78%. The pressure drop of the LCS porous Cu samples was measured in the same device, following the same procedure as used in the present study, so direct comparison can be made between LCS porous metals and microchannels. The conventional Cu microchannel [38] had a hydraulic diameter of 300 μm and sample length of 55 mm. It is shown that the pressure drops of the sintered Cu microchannels are higher than the conventional machined microchannel, but significantly lower than the LCS porous metals.

The machined microchannel has the lowest pressure drop because of the smooth internal surface of the microchannel and consequently low friction to the fluid flow. The LCS porous Cu has very high pressure drops because of the tortuous flow paths [29] and very rough surfaces along the flow paths (the maximum height of the profile would be 10 μm for the Cu powder used). The pressure drop in LCS porous metals is sensitive to porosity and decreases rapidly with porosity. At a low porosity, the pores are interlinked by fewer windows and the fluid pathways in the porous metal become restricted [39,40], leading to higher pressure drops. A high porosity means more inter-pore windows, less flow restrictions and therefore lower tortuosity [29], resulting in lower resistance to fluid flow. Although the sintered Cu microchannels have rough internal surface, the channels are straight and thicker than the effective channels in LCS porous metals. Overall, the flow resistance in the sintered microchannels is higher than the machined microchannels but is reduced considerably compared to LCS porous metals.

In an ideal condition, the pressure drop in microchannels can be described by the Darcy-Weisbach equation [41,42]:

$$\frac{\Delta p}{L} = f_D \cdot \frac{\rho}{2} \cdot \frac{v^2}{D} \tag{3}$$

where Δp is the pressure drop across the microchannel, L is the length of the microchannel, f_D is the Darcy friction factor, ρ is the density of the fluid, v is the flow velocity in the microchannel, and D is diameter of the channel. For laminar flows ($Re < 2300$), $f_D = 64/Re$ [42] and the Darcy-Weisbach equation becomes:

$$\frac{\Delta p}{L} = \frac{32\mu^2 Re}{\rho D^3} \tag{4}$$

where μ is the dynamic viscosity of the fluid and the Reynolds number is defined by [43,44]:

$$Re = \frac{\rho v D}{\mu} \tag{5}$$

Fig. 7 shows the relationships between pressure drop and Reynolds number for the sintered Cu microchannels with different volume fractions of channels (0.1, 0.2, 0.3 and 0.4) and different channel diameters (450 μm, 390 μm and 290 μm). The Reynolds number values as calculated by Eq. (5), with $\rho = 1000$ kg/m^3 and

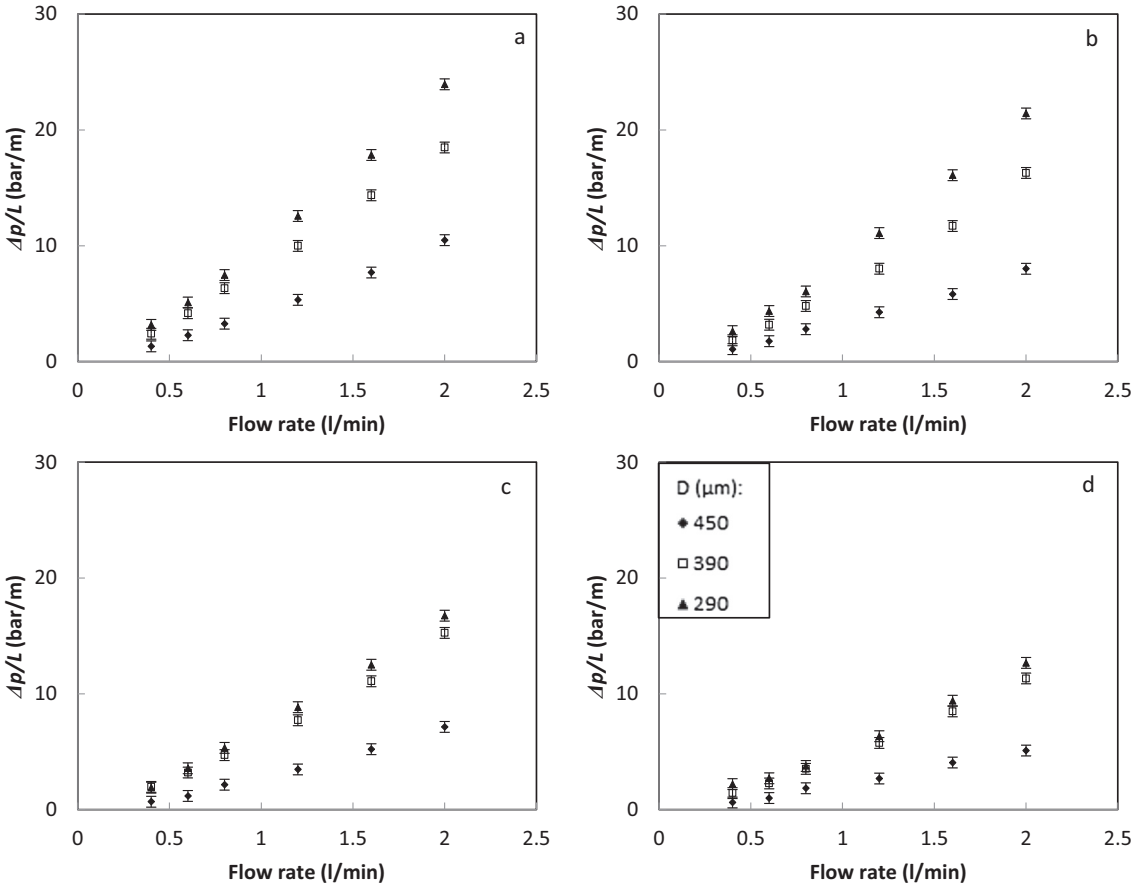

Fig. 5. Variations of pressure drop per unit length with flow rate for the sintered Cu microchannels with different volume fractions of channels (a) 0.1, (b) 0.2, (c) 0.3 and (d) 0.4. Channel diameters (◆ 450 μm, □ 390 μm, ▲ 290 μm).

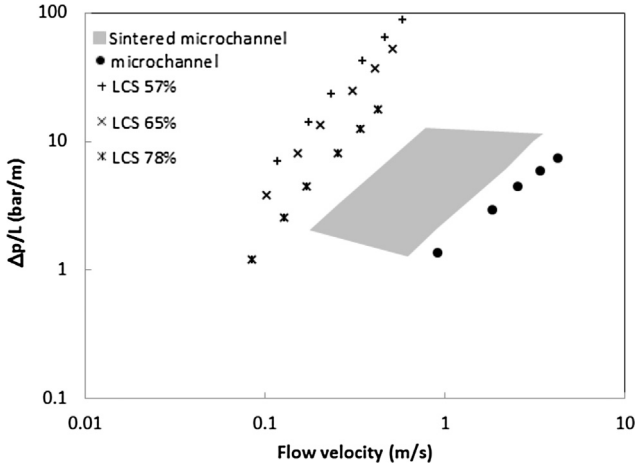

Fig. 6. Comparisons of pressure drops as a function of flow velocity between the sintered Cu microchannels (shaded area), the LCS porous Cu [37] and a machined Cu microchannel [38].

μ = 0.001136 Ns/m^2 for water, are less than 1320, so the fluid flow in the sintered microchannels can be considered as fully laminar. The theoretical predictions based on Eq. (4) are also presented in Fig. 7 for comparison purposes.

Fig. 7 shows that the pressure drop has a good linear relation with *Re* for all the samples and increases with decreasing channel diameter, qualitatively in agreement with the theoretical predictions. However, the experimental pressure drop values are considerably (50%–100%) higher than the theoretical values. This can be explained by the fact that the microchannels, formed by sintering Cu particles, have rough channel walls and therefore much higher flow resistance values than the theoretical values assumed for smooth surfaces.

It should be noticed that, for any given channel diameter, the experimental pressure drop at any fixed *Re* value increases with increasing volume fraction of channels, while theoretically pressure drop should not be affected by volume fraction of channels (see Eq. (4)). This anomaly is due to the entrance effect experienced in the tests. The fluid initially flows across the whole cross section of the sample and is then forced to enter the channels with a much reduced cross sectional area. A higher pressure is required to overcome the resistance presented by the entrance region, which is expected to be proportional to the circumference of the channel for each channel. For a fixed channel diameter, the higher the volume fraction of channels, the larger the circumferences of the channels and thus the higher the extra resistance due to the entrance effect.

In addition to the surface roughness and entrance effects, two more factors may also have contributed to the deviations in pressure drop from ideal microchannels. First, the flow in the sintered microchannels is in the developing regime rather than fully developed. Second, there are numerous small pores in the metal matrix, formed between the metal particles due to incomplete sintering, as shown in Fig. 2. Although flow resistance in the porous Cu matrix (approximately 15% porosity) is much higher than the channels, some water can still flow through these small pores.

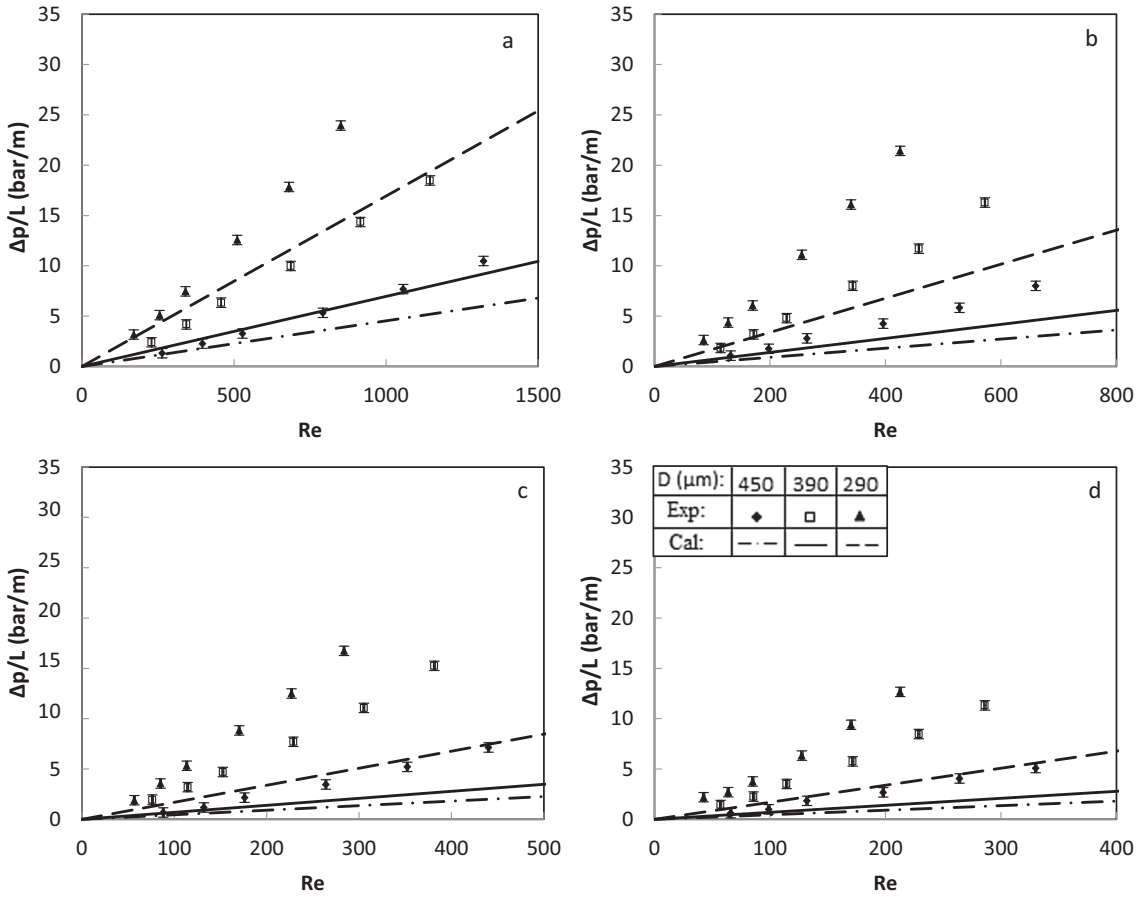

Fig. 7. Variations of pressure drop with Reynold number for the sintered Cu microchannels with volume fraction of channels: (a) 0.1, (b) 0.2, (c) 0.3 and (d) 0.4, in comparison to Darcy-Weisbach predictions, for different channel diameters.

3.2. Heat transfer coefficient

Fig. 8 shows the variations of heat transfer coefficient with flow rate for the sintered Cu microchannels with different volume fractions of channels (0.1, 0.2, 0.3 and 0.4) and different channel diameters (450 μm, 390 μm and 290 μm). It shows that the heat transfer coefficient increases with flow rate, increases with volume fraction of channels and decreases with channel diameter. Increasing fluid flow rate and/or volume fraction of channels increases the convective heat transfer through the fluid. With fixed fluid flow rate and volume fraction of channels, a smaller channel diameter means that the microchannels have a higher total internal surface area, promoting heat transfer between the metal matrix and the fluid. However, it should be noted that the effects of volume fraction of channels and channel diameter on heat transfer coefficient are less pronounced than those on pressure drop. This is because heat transfer depends not only on convection by the flow in the channels but also on conduction in the metal matrix. Increasing volume fraction of channels increases convection but decreases conduction. Given a fixed volume fraction of channels, varying channel diameter does not affect both conduction and convection, although it changes the interfacial area between the metal matrix and the liquid flow and therefore affects the heat transfer at the interface to some extent.

Fig. 9 compares heat transfer coefficients of the sintered Cu microchannels with those of the LCS porous Cu [37] and a conventionally machined Cu microchannel [45], as a function of flow velocity. The areal volumes of channels of the sintered Cu microchannels are 0.5 mm, 1.0 mm, 1.5 mm and 2.0 mm, corresponding to volume fractions of 0.1, 0.2, 0.3 and 0.4, respectively. The equivalent areal volumes of channels of the LCS porous Cu are 2.85 mm, 3.25 mm and 3.9 mm, corresponding to the porosities of 57%, 65% and 78%, respectively. The heat transfer coefficient of the LCS porous Cu samples was measured in the same device, following the same procedure as used in the present study, so direct comparison can be made between LCS porous metals and microchannels. The conventional Cu microchannel [45] had a hydraulic diameter of 281 μm and an areal volume of channels of 0.2 mm.

Fig. 9 shows that the heat transfer coefficients of the sintered Cu microchannels vary in a wide range, with the lower bound comparable to that of the conventional machined microchannel and the upper bound comparable to the highest heat transfer coefficient achieved in the LCS porous metals. The main advantage of the sintered microchannels over the conventional microchannels is that multilayers of channels can be embedded in the metal matrix, while the conventional microchannels only have one layer of channels. This results in a considerably higher areal volumes of channels in the sintered microchannels (0.5–2 mm vs 0.2 mm), which is main reason for the better heat transfer performance of the sintered Cu microchannels than their conventional counterparts. The high areal volume of channels of sintered microchannels can easily compensate the reduced thermal conductivity in the porous metal matrix.

The sintered Cu microchannels achieved a similar range of heat transfer coefficients as the LCS porous Cu with much lower areal volumes of channels (0.5–2 mm vs 2.85–3.9 mm). The LCS porous Cu has a microstructure (Fig. 1) very different from microchannels.

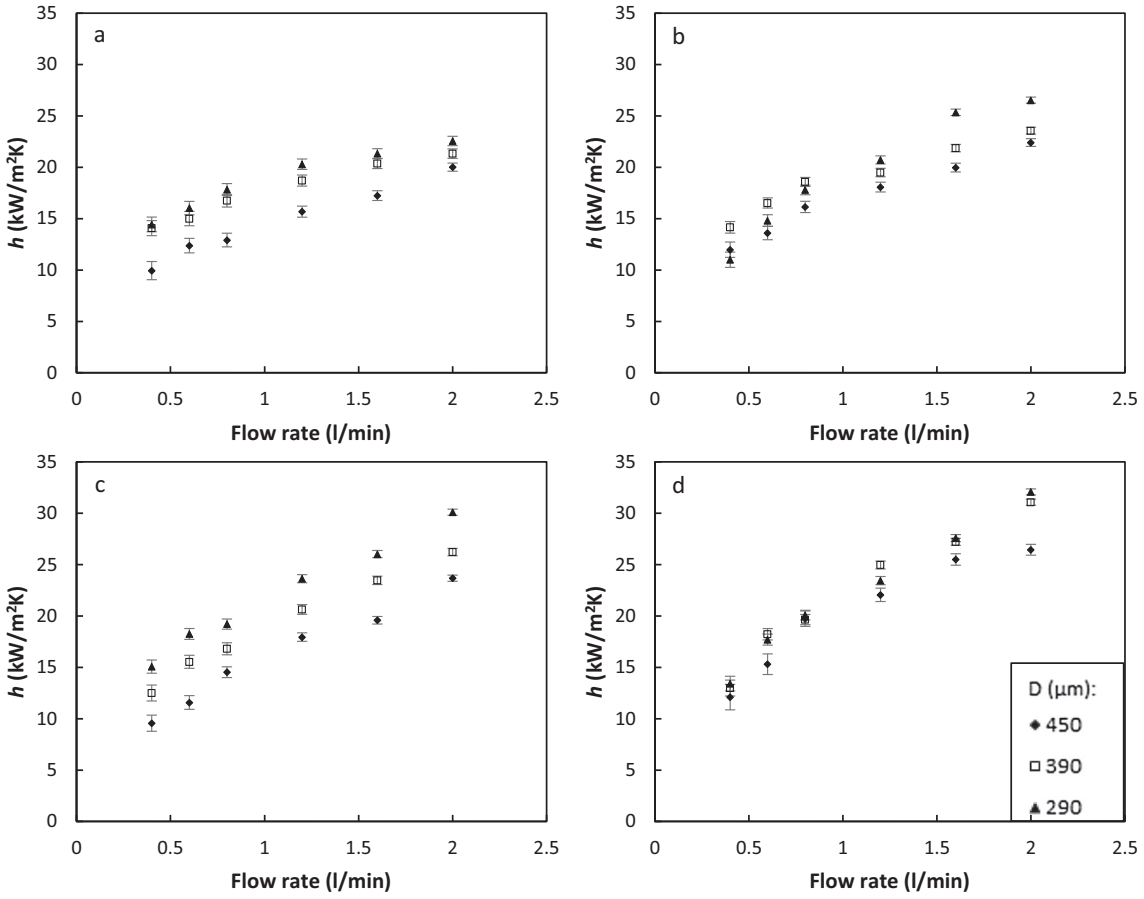

Fig. 8. Variations of heat transfer coefficient with flow rate for the sintered Cu microchannels with different volume fractions of channels (a) 0.1, (b) 0.2, (c) 0.3 and (d) 0.4. Channel diameters (◆ 450 μm, □ 390 μm and ▲ 290 μm).

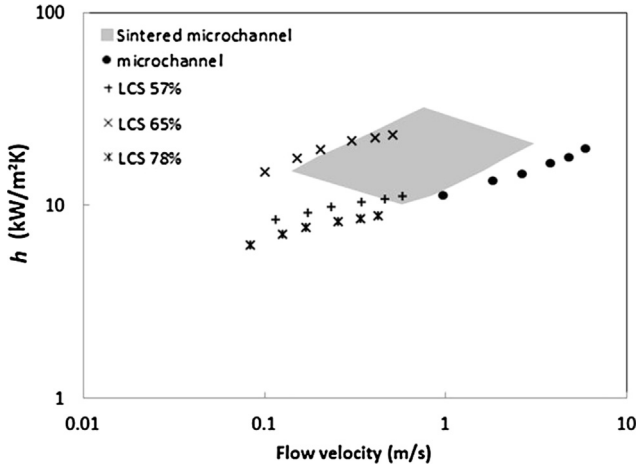

Fig. 9. Comparisons of heat transfer coefficients as a function of flow velocity between the sintered Cu microchannels (shaded area), the LCS porous Cu [37] and a machined Cu microchannel [45].

In conventional microchannels, the metal matrix is fully dense. The heat transfer is usually limited by convection in the fluid flow in the channels and is therefore sensitive to the areal volume of channels. The LCS porous Cu not only contains large, interconnected primary pores (primary porosity) that serve as flow channels, but also has numerous voids in the metal matrix (secondary porosity) that reduce the thermal conduction in the metal matrix. The heat transfer coefficient is very sensitive to porosity. At a low porosity, thermal conduction in the matrix is high, but convection by the fluid flow is reduced due to less flow channels. At a high porosity, on the other hand, there are many flow channels for convection, while the poor conduction of the matrix becomes the bottleneck for overall heat transfer. The best heat transfer performance is achieved at an intermediate porosity of 65%, at which the conduction in the metal matrix matches the convection in the fluid flow and an optimum overall heat transfer is resulted [46]. The sintered Cu microchannels can be seen as an intermediate structure between conventional Cu microchannels and LCS porous Cu. For the same heat transfer coefficient, their pressure drop is much lower than the LCS metals as shown previously in Fig. 6. For a similar pressure drop, their heat transfer coefficient can be significantly higher than the conventional microchannels.

For laminar flow ($Re < 2300$), Nusselt number of a single channel, Nu_s, can be expressed by the Sieder-Tate equation [47]:

$$Nu_s = 1.86 Re^{\frac{1}{3}} Pr^{\frac{1}{3}} \left(\frac{D}{L}\right)^{\frac{1}{3}} \left(\frac{\mu}{\mu_s}\right)^{0.14} \tag{6}$$

where Pr is the Prandtl number, μ_s is the dynamic viscosity of the fluid evaluated at the channel wall temperature, and the Nusselt number of a single channel is defined as [48]:

$$Nu_s = \frac{h_s D}{k} \tag{7}$$

where h_s is the heat transfer coefficient between the channel wall and the fluid, and k is the thermal conductivity of the fluid.

The heat transfer coefficient of the sintered Cu microchannels, h, however, is defined differently from that of a single channel,

h_s. In the experiments, the area used to calculate the heat transfer coefficient is the area of the sample in contact with the heating block ($A = xL$), instead of the total area of the channel in contact with the fluid ($A_s = N\pi DL$). Appreciating that the ratio between the volume and surface area of cylindrical channels is $D/4$, the heat transfer coefficient of the sintered Cu microchannels is therefore related to the heat transfer coefficient of a single channel by:

$$h = \frac{A_s}{A} h_s = \frac{4V_A}{D} h_s \tag{8}$$

In other words, the heat transfer coefficient of the sintered Cu microchannels is dependent not only on the heat transfer coefficient of individual channels, but also on the areal volume of the channels and the channel diameter.

As a consequence, the Nusselt number of the sintered Cu microchannels, Nu, is also defined differently from that of a single channel, Nu_s, and they are related by:

$$Nu = \frac{4V_A}{D} Nu_s \tag{9}$$

The Sieder-Tate equation, Eq. (6), can therefore be expressed in terms of Nu and re-arranged to give:

$$Nu = 7.44 V_A D^{-\frac{2}{3}} L^{-\frac{1}{3}} \left(\frac{\mu}{\mu_s}\right)^{0.14} Pr^{\frac{1}{3}} Re^{\frac{1}{3}} \tag{10}$$

Fig. 10 shows the relationships between Nusselt number and Reynolds number for the sintered Cu microchannels with different volume fractions of channels (0.1, 0.2, 0.3 and 0.4) and different channel diameters (450 μm, 390 μm and 290 μm). The theoretical predictions based on Eq. (10) are also presented in Fig. 10 for comparison purposes. The physical properties of water used in the calculations are: $Pr = 7.56$, $\mu = 0.001136$ Ns/m^2 (15 °C at water inlet) and $\mu_s = 0.000955$ Ns/m^2 (22 °C at channel wall).

Fig. 10 shows that the Nusselt number is nearly proportional to the areal volume of channels, in good agreement with Eq. (10). The relationships between the Nusselt number and Re are also qualitatively in agreement with the theoretical predictions. However, the Nusselt number is proportional to $Re^{0.33}$, $Re^{0.38}$, $Re^{0.45}$ and $Re^{0.53}$ (according to the fitted lines in Fig. 10), for volume fractions of channels of 0.1, 0.2, 0.3 and 0.4, or areal volumes of channels of 0.5 mm, 1.0 mm, 1.5 mm and 2.0 mm, respectively. The exponent on Re increased with areal volumes of channels, instead of a constant value of 1/3 as predicted in an ideal microchannel. In other words, the heat transfer coefficient of the sintered Cu microchannel with a higher areal volume increased with flow velocity more rapidly. The effect of channel diameter on the Nusselt number is hardly discernible, although the Sieder-Tate equation, Eq. (6), predicts that reducing channel diameter from 450 μm to 390 μm and to 290 μm could result in reductions in the Nusselt number by 5% and 16%, respectively.

Quantitatively, however, the experimental values of the Nusselt number are one order of magnitude lower than the theoretical predictions, being approximately 28%, 18%, 15% and 13% of the predicted values corresponding to the areal volumes of channels of 0.5 mm, 1.0 mm, 1.5 mm and 2.0 mm, respectively. The large differences between the experimental and theoretical values can be attributed to several factors. Firstly, the metal matrix in the sintered Cu microchannels is porous instead of solid. With a porosity

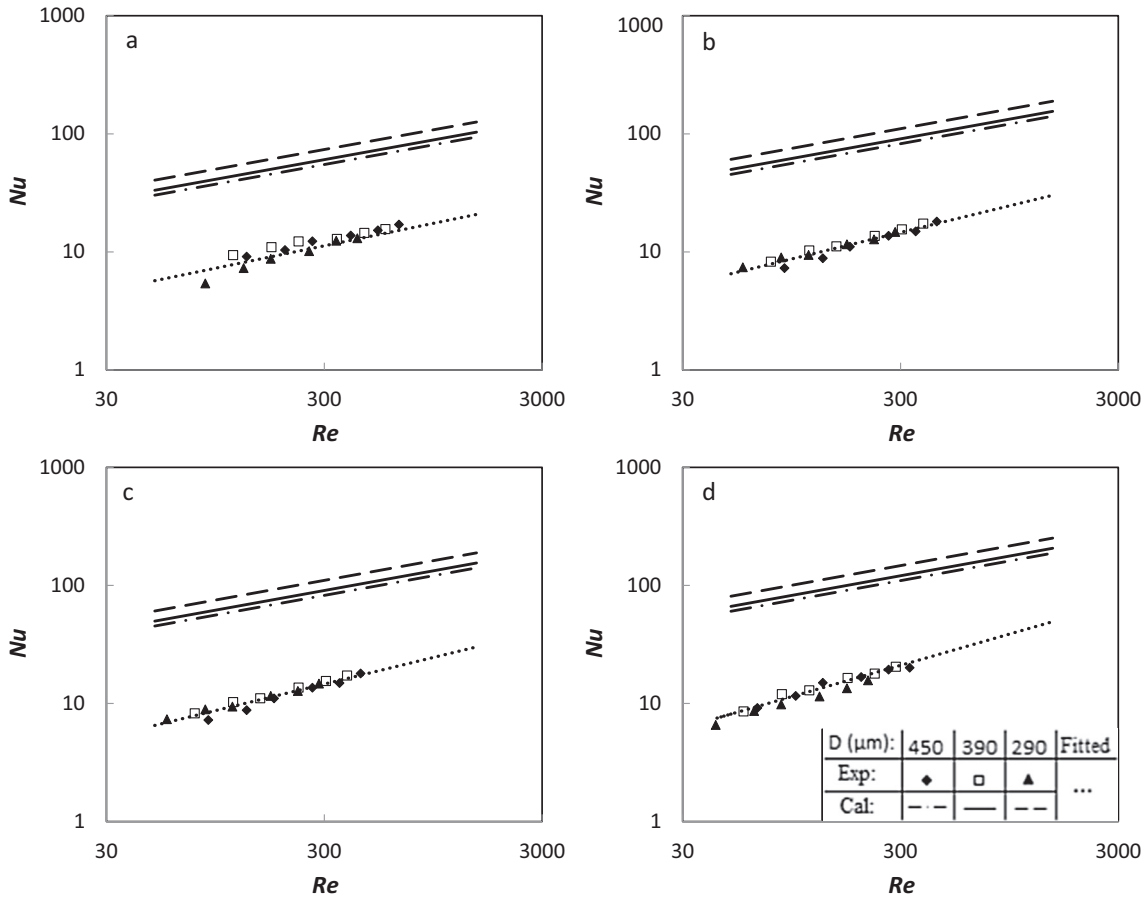

Fig. 10. Variations of Nuselt number (Nu) with Reynold number (Re) for the sintered Cu microchannels with volume fraction of channels: (a) 0.1, (b) 0.2, (c) 0.3 and (d) 0.4 (areal volume of channels: (a) 0.5 mm, (b) 1.0 mm, (c) 1.5 mm and (d) 2.0 mm), in comparison to Sieder-Tate predictions, for different channel diameters.

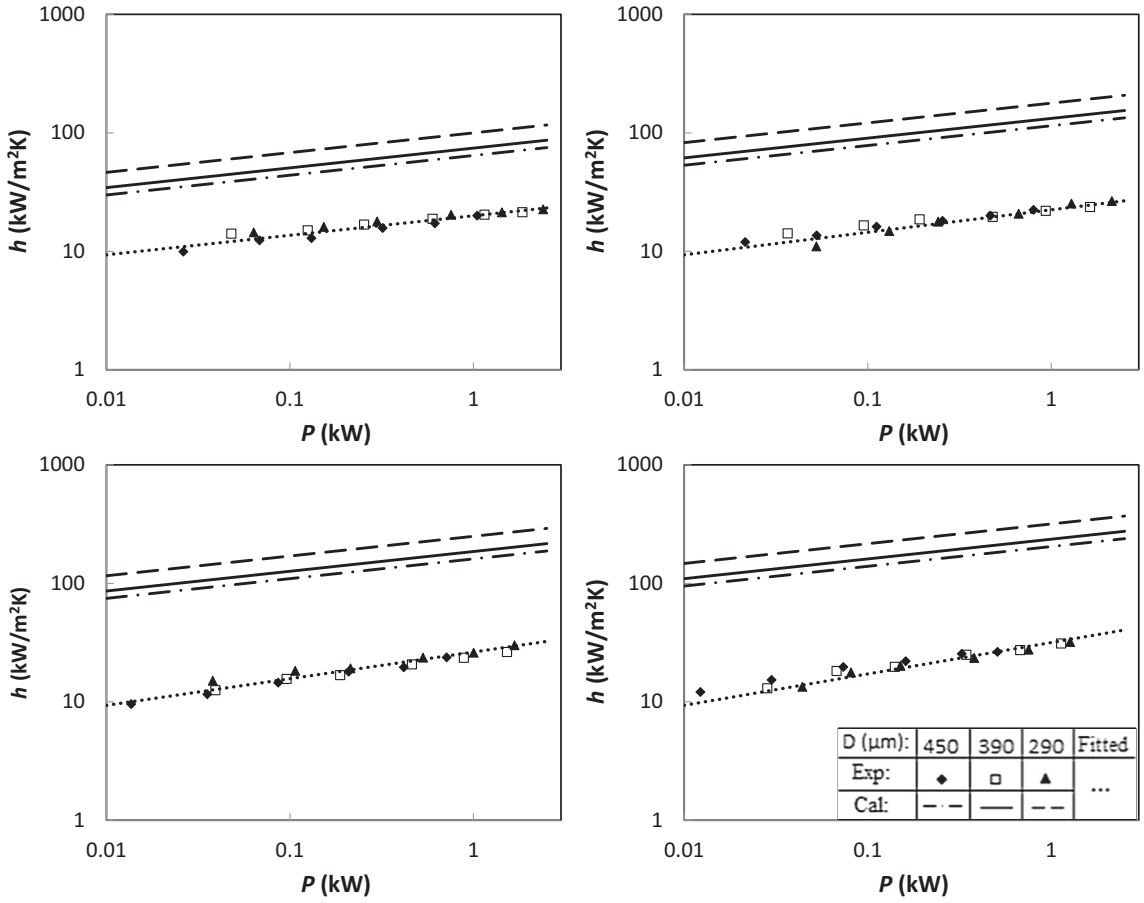

Fig. 11. Relationship between heat transfer coefficient (h) and pumping power (P) for the sintered Cu microchannels with volume fraction of channels: (a) 0.1, (b) 0.2, (c) 0.3 and (d) 0.4 (areal volume of channels: (a) 0.5 mm, (b) 1.0 mm, (c) 1.5 mm and (d) 2.0 mm), in comparison to theoretical predictions, for different channel diameters.

of 15%, its thermal conductivity is approximately 70% of that of solid Cu [49]. Secondly, the microchannels have rough and porous walls, so the convectional heat transfer coefficient at the channel wall/fluid interface may be considerably different from that in a conventional channel with smooth solid surfaces. Thirdly, the theoretical expression of the Nusselt number, Eq. (10), was developed based on the relation between the heat transfer coefficient of the sintered Cu microchannels and the heat transfer coefficient of a single channel, Eq. (8), which is valid only if no temperature gradient exists in the metal matrix and the temperature difference between the channel wall and the fluid remains the same in all the channels. This is not true in sintered Cu microchannels, because there is a temperature gradient along the direction of heat flow (y direction in Fig. 4) due to the finite thermal conductivity of the porous Cu matrix. The temperature difference between the channel wall and the fluid depends on the location of the channel, decreasing as the channel is located further away from the heat source. The channels far away from the heat sources remove less heat than those close to the heat sources, leading to an over-prediction by Eq. (10).

3.3. Relationship between heat transfer coefficient and pumping power

Pumping power is another important consideration for active cooling. In the assessment of the overall heat transfer performance of any heat exchangers, both heat transfer coefficient and pumping requirement need to be taken into account.

For microchannels, the pumping power required for moving the fluid through the channels, P, is the product of the pressure drop, Δp, and the volume flow rate of the fluid, U. Appreciating that the total cross sectional area of the channels for the fluid to pass through is related to the areal volume of the channels by AV_A/L, the pumping power can be expressed in terms of flow velocity by:

$$P = \Delta p \times U = \Delta p \frac{AV_A}{L} v \tag{11}$$

As the pressure drop in microchannels is calculated by the Darcy-Weisbach equation, Eq. (4), the pumping power can be expressed in terms of the flow velocity by:

$$P = \frac{32\rho\mu AV_A}{D^2} v^2 \tag{12}$$

The heat transfer coefficient of the sintered Cu microchannels can be directly obtained from the Nusselt number, which is calculated by the Sieder-Tate equation, Eq. (10). Therefore, the heat transfer coefficient can also be expressed in terms of the flow velocity by:

$$h = \frac{kNu}{D} = 7.44 V_A D^{-\frac{4}{3}} L^{-\frac{1}{3}} k \left(\frac{\mu}{\mu_s}\right)^{0.14} \left(\frac{\rho Pr}{\mu}\right)^{\frac{1}{3}} v^{\frac{1}{3}} \tag{13}$$

Combining Eqs. (12) and (13) and eliminating the flow velocity term, the theoretical relationship between the heat transfer coefficient and pumping power can be obtained as:

$$h = 2.34 k \left(\frac{\mu}{\mu_s}\right)^{0.14} \left(\frac{\rho Pr^2}{\mu^3}\right)^{\frac{1}{6}} \frac{1}{D} \left(\frac{V_A^5}{AL^2}\right)^{\frac{1}{6}} P^{\frac{1}{6}} \tag{14}$$

The relationship is clearly affected by the fluid properties and the test specimen geometries. Given a fixed geometry and fluid, the heat transfer coefficient can be improved efficiently by increasing the areal volume of the channels, V_A. Increasing flow rate is not particularly effective for improving heat transfer performance because of the accompanied increase in pumping power. To double the heat transfer coefficient will result in an increase of 64 times in pumping power.

Fig. 11 shows the experimental and predicted relationships between heat transfer coefficient (h) and pumping power (P) for the sintered Cu microchannels with different volume fractions, or areal volumes, of channels and channel diameters. The relationships between h and P are qualitatively in good agreement with the theoretical predictions, with h being proportional to $P^{0.165}$, $P^{0.19}$, $P^{0.225}$ and $P^{0.265}$ (according to the fitted lines in Fig. 11), for volume fractions of channels of 0.1, 0.2, 0.3 and 0.4, or areal volumes of channels of 0.5 mm, 1.0 mm, 1.5 mm and 2.0 mm, respectively, instead of $P^{1/6}$ as predicted. Quantitatively, however, there is a large difference between the experimental and predicted values, mainly due to the large difference in the pressure drops between the sintered and conventionally machined microchannels. A correcting factor needs to be introduced to accounting for the difference, if Eq. (14) is to be used in any predictions. It is worth noting that the relationship between h and P is insensitive to channel diameter.

4. Conclusions

(1) Cu microchannels with well controlled channel diameters (450 μm, 390 μm and 290 μm) and volume fractions of channels (0.1, 0.2, 0.3 and 0.4), corresponding to different areal volumes of channels (0.5 mm, 1.0 mm, 1.5 mm and 2.0 mm), have been manufactured by a new sintering method. Their pressure drops and heat transfer coefficients under a range of water flow rate have been measured.

(2) The pressure drops of the sintered Cu microchannels are higher than the conventional machined microchannel, but significantly lower than the LCS porous metals. The pressure drops are higher than the theoretical values predicted for an ideal microchannel, due to strong frictions at rough channel walls and the entrance effect.

(3) The sintered Cu microchannels achieved a similar range of heat transfer coefficients as the LCS porous Cu, with much lower volume fractions of channels. The heat transfer coefficients of the sintered Cu microchannels are higher than the conventional machined microchannel mainly due to the introduction of multilayers of channels in the metal matrix.

(4) The pressure drop and heat transfer coefficient of the sintered Cu microchannels can be described by the Darcy-Weisbach and Sieder-Tate equations with the introduction of appropriate correcting factors. There is a strong correlation between heat transfer coefficient and pumping power.

Conflict of interest

The authors declare that there is no conflict of interest regarding the publication of this article.

Acknowledgment

This work has been supported by the Engineering and Physical Sciences Research Council (Grant No. EP/N006550/1).

Appendix A. Supplementary material

Supplementary data to this article can be found online at https://doi.org/10.1016/j.ijheatmasstransfer.2019.05.020.

References

[1] R. Mahajan, R. Nair, V. Wakharkar, J. Swan, J. Tang, G. Vandentop, Emerging directions for packaging technologies, Intel Technol. J. 6 (2002) 62.
[2] H. Zhang, Y. Liu, Y. Li, L. Chen, Experimental study on heat transfer performance of lotus-type porous copper heat sink, Int. J. Heat Mass Transfer. 56 (2013) 172–180.
[3] M. Wong, I. Owen, C. Sutcliffe, A. Puri, Convective heat transfer and pressure losses across novel heat sinks fabricated by selective laser melting, Int. J. Heat Mass Transfer 52 (2009) 281–2888.
[4] G. Morini, Review article: Single-phase convective heat transfer in microchannels: a review of experimental results, Int. J. Therm. Sci. 43 (2004) 631–651.
[5] M. Ohadi, K. Choo, S. Dessiatoun, E. Cetegen, Next Generation Microchannel Heat Exchangers, Springer, New York, 2013.
[6] S. Prakash, S. Kumar, Fabrication of microchannels: A review, Proc. Inst. Mech. Eng. Pt. B: J. Eng. Manuf. 229 (2015) 1273–1288.
[7] C. Sobhan, S. Garimella, A comparative analysis of studies on heat transfer and fluid flow in microchannels, Microsc. Therm. Eng. (2001) 293.
[8] N. Obot N, Toward a better understanding of friction and heat/mass transfer in microchannels - A literature review, Microsc. Therm. Eng. 6 (2002) 155–173.
[9] M. Khan, A. Fartaj, A review on microchannel heat exchangers and potential applications, Int. J. Energy Res. 35 (2011) 553–582.
[10] M. Ashby, Metal Foams: A Design Guide, Butterworth-Heinemann, Boston, 2000.
[11] L. Gibson, M. Ashby, Cellular Solids: Structure and Properties, Pergamon, Oxford, 1988.
[12] J. Baloyo, Y. Zhao, Heat transfer performance of micro-porous copper foams with homogeneous and hybrid structures manufactured by lost carbonate sintering, MRS Proc. 1779 (2015), mrss 15-2095240.
[13] Z. Xiao, Y. Zhao, Heat transfer coefficient of porous copper with homogeneous and hybrid structures in active cooling, J Mater. Res. 28 (2013) 2545–2553.
[14] Y. Qin, Micro-manufacturing Engineering and Technology, Elsevier, Boston, 2010.
[15] M. Pan, D. Zeng, Y. Tang, Feasibility investigations on multi-cutter milling process: A novel fabrication method for microreactors with multiple microchannels, J. Power Sources 192 (2009) 562–572.
[16] Z. Wan, Y. Li, H. Tang, W. Deng, Y. Tang, Characteristics and mechanism of top burr formation in slotting microchannels using arrayed thin slotting cutters, Precis. Eng. 38 (2014) 28–35.
[17] M. Madou, Fundamentals of Microfabrication: The Science of Miniaturization, CRC Press, Boca Raton, 2002.
[18] J. Brugger, R. Buser, N. de Rooij, Silicon cantilevers and tips for scanning force microscopy, Sens. Actuators A Phys. 34 (1992) 193–200.
[19] T. Kikuchi, Y. Wachi, M. Sakairi, R. Suzuki, Aluminum bulk micromachining through an anodic oxide mask by electrochemical etching in an acetic acid/perchloric acid solution, Microelectron. Eng. 111 (2013) 14–20.
[20] J. Park, N. Lee, J. Lee, J. Park, H. Park, Deep dry etching of borosilicate glass using SF6 and SF6/Ar inductively coupled plasmas, Microelectron. Eng. 82 (2005) 119–128.
[21] V. Maselli, R. Osellame, G. Cerullo, R. Ramponi, P. Laporta, L. Magagnin, Fabrication of long microchannels with circular cross section using astigmatically shaped femtosecond laser pulses and chemical etching, Appl. Phys. Lett. 88 (2006).
[22] J. Cheng, C. Liu, S. Shang, D. Liu, W. Perrie, G. Dearden, A review of ultrafast laser materials micromachining, Opt. Laser. Technol. 46 (2013) 88–102.
[23] E. Gamaly, A. Rode, B. Luther-Davies, V. Tikhonchuk, Ablation of solids by femtosecond lasers: Ablation mechanism and ablation thresholds for metals and dielectrics, Phys. Plasmas. 949 (2002).
[24] K. Sokolowski-Tinten, J. Bialkowski, A. Cavalleri, dL. Von, A. Oparin, J. Meyer-ter-Vehn, Transient states of matter during short pulse laser ablation, Phys. Rev. Lett. 81 (1998) 224–227.
[25] Y. Zhao, D. Sun, A novel sintering-dissolution process for manufacturing Al foams, Scr. Mater. 44 (2001) 105.
[26] Y. Zhao, T. Fung, L. Zhang, F. Zhang, Lost carbonate sintering process for manufacturing metal foams, Scr. Mater. 52 (2005) 295–298.
[27] G. Zaragoza, R. Goodall, Development of a device for the measurement of thermal and fluid flow properties of heat exchanger materials, Measurement 56 (2014) 37–49.
[28] P. Langston, A. Kennedy, Discrete element modelling of the packing of spheres and its application to the structure of porous metals made by infiltration of packed beds of NaCl beads, Powder Technol. 268 (2014) 210–218.
[29] K. Diao, L. Zhang, Y. Zhao, Measurement of tortuosity of porous Cu using a diffusion diaphragm cell, Measurement 110 (2017) 335–338.
[30] G. Jiang, Y. Li, Y. Liu, Experimental study on the pore structure of directionally solidified porous Cu-Mn alloy, Metall. Mat. Trans. A Phys. Metall. Mat. Sci. 41 (2010) 3405–3411.

[31] G. Jiang, Y. Li, Y. Liu, Influence of solidification mode on pore structure of directionally solidified porous Cu-Mn alloy, Trans. Nonferrous. Met. Soc. China. 21 (2011) 88–95.
[32] L. Yuan, L. Yanxiang, W. Jiang, Z. Huawei, Evaluation of porosity in lotus-type porous magnesium fabricated by metal/gas eutectic unidirectional solidification, Mater. Sci. Eng. A. 402 (2005) 47–54.
[33] H. Nakajima, Fabrication, properties, and applications of porous metals with directional pores, Prog. Mater. Sci. 52 (2007) 1091–1173.
[34] V. Shapovalov, Porous metals, MRS Bull. 19 (1994) 24–28.
[35] M. Jin, Y. Qu, J. You, R. Li, Casting of array micro-holes on Al components, Int. J. Adv. Manuf. Technol. 81 (2015) 1017–1021.
[36] K. Hokamoto, M. Vesenjak, Z. Ren, Fabrication of cylindrical uni-directional porous metal with explosive compaction, Mater. Lett. 137 (2014) 323–327.
[37] K. Diao, X. Lu, Z. Wu, Y. Zhao, Heat Transfer performance of LCS porous copper with different structural characteristics, Mater. Sci. Forum 933 (2018) 380–387.
[38] H. Cao, G. Chen, Q. Yuan, Thermal performance of crossflow microchannel heat exchangers, Ind. Eng. Chem. Res. 49 (2010) 6215–6220.
[39] W. Zhou, Q. Qiu, J. Tu, Q. Wang, Y. Tang, K. Hui, Heat and mass transfer characterization of porous copper fiber sintered felt as catalyst support for methanol steam reforming, Fuel 145 (2015) 136–142.
[40] W. Zhou, Y. Tang, M. Pan, X. Wei, J. Xiang, H. Chen, A performance study of methanol steam reforming microreactor with porous copper fiber sintered felt as catalyst support for fuel cells, Int. J. Hydrogen Energy. 34 (2009) 9745–9753.
[41] T. Hughes, R. Jeppson, Hydraulic friction loss in small diameter plastic pipelines, J. Am. Water Resour. Assoc. 14 (1978) 1159.
[42] F. Incropera, Fundamentals of Heat and Mass Transfer, John Wiley, Hoboken, NJ, 2007.
[43] O. Reynolds, An experimental investigation of the circumstances which determine whether the motion of water shall he direct or sinuous, and of the law of resistance in parallel channels, Phil. Trans. R. Soc. Lond. 174 (1884) 935–982.
[44] K. Avila, D. Moxey, dL. Alberto, M. Avila, D. Barkley, H. Björn, The onset of turbulence in pipe flow, Science (2011) 192.
[45] B. Lu, K. Chen, W. Meng, F. Mei, Fabrication, assembly and heat transfer testing of low-profile copper-based microchannel heat exchangers, J. Micromech. Microeng. 20 (2010).
[46] L. Zhang, D. Mullen, K. Lynn, Y. Zhao, Heat transfer performance of porous copper fabricated by the lost carbonate sintering process, Mater. Res. Soc. Symp. Proc. 1188 (2009) 7.
[47] J. Welty, C. Wicks, R. Wilson, Fundamentals of Momentum, Heat, and Mass Transfer, Wiley, New York, 1969.
[48] E. Sanvicente, S. Giroux-Julien, C. Ménézo, H. Bouia, Transitional natural convection flow and heat transfer in an open channel, Int. J. Therm. Sci. 63 (2013) 87–104.
[49] D. Thewsey, Y. Zhao, Thermal conductivity of porous copper manufactured by the lost carbonate sintering process, Phys. Status Solidi. A 205 (2008) 1126–1131.